Characteristics of the TPE Reversed-Field Pinch Plasmas in Conventional and Improved Confinement Regimes

H. Sakakita 1), Y. Yagi 1), T. Asai 2), G. Fiksel 3), L. Frassinetti 1), K. Hayase 1), Y. Hirano 1), P. Innocente 4), S. Kiyama 1), H. Koguchi 1), Y. Sato 5), T. Shimada 1), G. Spizzo 4), D. Terranova 4), M. Yoshikawa 6)

1) National Inst. of Advanced Industrial Science and Tech. (AIST), Tsukuba 305-8568, Japan
2) Nihon University, Tokyo 101-8308, Japan
3) University of Wisconsin – Madison, Madison, WI 53706, USA
4) Consorzio RFX, I-35127 Padua, Italy
5) Tokyo Metropolitan College of Technology, Tokyo 140-0011, Japan
6) University of Tsukuba, Tsukuba 305-8577, Japan

e-mail contact of main author: h.sakakita@aist.go.jp

Abstract. We present the characteristics and experimental scaling laws of reversed-field pinch (RFP) plasmas, which are obtained from the recently established toroidal pinch experiment (TPE) database. The database contains information for approximately 1500 discharges consistently selected from four TPE RFP devices, and covers two decades of RFP experiments under conventional operating conditions at the National Institute of Advanced Industrial Science and Technology. We present the physics of the pulsed poloidal current drive (PPCD) discharges in the TPE-RX RFP device, and a comparison of the improved energy confinement time in PPCD, τ_{E_PPCD}, with $\tau_{E\_scaling}$ as the reference scaling law ($\tau_{E\_scaling} \sim a^{1.63} I_P^{0.78} (I_P/N)^{0.33} \Theta^{2.97}$) in the TPE database, is attempted. The result shows that τ_{E_PPCD} agrees well with $\tau_{E\_scaling}$ because of the strong pinch parameter dependence on the TPE scaling law. A potential improved confinement mode in the quasi-single-helicity (QSH) state is also investigated in TPE-RX, with respect to the operation conditions under which the QSH spontaneously appears in the core region, where a typical island structure is observed by means of soft X-ray tomography.

1. Introduction

Over the past two decades, the global confinement characteristics for many reversed-field pinch (RFP) devices have been studied, and scaling laws in RFP have been analyzed [1-3]. Regarding scaling study, it is important to confirm the energy confinement time, τ_E, to follow what kind of scaling, e.g., constant-β_P scaling [4] limited by a resistive interchange mode, scaling limited by tearing instability [5,6] or another type of scaling (β_p denotes the poloidal beta). The optimum τ_E values for the most well known RFP devices approximately follow constant-β_P scaling. On the other hand, it has been shown that improved confinement has been obtained by the pulsed poloidal current drive (PPCD) method [7] in many RFP devices. It is also important to confirm the degree of improvement in PPCD, and to compare τ_E in PPCD with the τ_E scaling law under conventional conditions.

In the present paper, the result of regression analysis using the toroidal pinch experiment (TPE) database [8] is described (Section 2), and the resultant scaling law is compared with the improved confinement time in PPCD to estimate the degree of improvement (Section 3) [9]. Also, the operating conditions necessary to obtain a higher PPCD performance are analysed. The quasi-single-helicity (QSH) state, which has a potential improved confinement mode, is also investigated in TPE-RX with respect to the operation conditions under which the QSH spontaneously appears (Section 4) [10].

2. Scaling Law of RFP Confinement in TPE Database

A database of the confinement properties in four TPE RFP plasmas has recently been established [8]. The database, called the TPE database, contains information for approximately 1500 discharges, and covers two decades of RFP experiments under conventional operating conditions at the National Institute of Advanced Industrial Technology (and the former Electrotechnical Laboratory) in Tsukuba; the discharges were consistently selected from TPE-1RM (R/a = 0.5/0.09 m, since 1980), TPE-1RM15 (R/a = 0.70/0.135 m, since 1985), TPE-1RM20 (R/a = 0.75/0.192 m, since 1992), and TPE-RX (R/a = 1.72/0.45 m, the present device, in use since 1998), where R and a are the major and minor radii of the plasma, respectively. The TPE database is characterized by relatively high I_P/N values ranging from 5 to 40 x 10^{-14} Am, where I_P is the plasma current, $N = \pi a^2 \langle n_e \rangle$, and $\langle n_e \rangle$ is the volume averaged electron density. Note that I_P and I_P/N can be independently operated in RFP, although n_e is proportional to I_P under standard prefuelling of the working gas. The conventional operation does not include active methods of obtaining improved confinement such as PPCD, and this means that the RFP was obtained under optimised equilibrium conditions as well as with the minimized error field at the shell gap, the deuterium gas was supplied well in advance of the discharges, and active gas feeding using gas puffing or pellet injection during the discharges was not included. However, the data for the improved high-theta mode (IHTM) in TPE-1RM20 [11], which was a spontaneously improved confinement state, is included in the TPE database.

Regression analysis for the shot-averaged τ_E database obtained from I_P and F/Θ scanning ($F = B_t(a)/\langle B_t \rangle$ and $\Theta = B_\theta(a)/\langle B_t \rangle$, $B_t(a)$ and $B_\theta(a)$ being the toroidal and poloidal magnetic fields at $r = a$, respectively, and $\langle B_t \rangle$ the volume-averaged toroidal magnetic field) provides scaling laws for β_p and τ_E, as shown in FIG. 1. The scaling of β_p is obtained by substituting result of scaling the core electron temperature, T_{e0}, into the definition of $\beta_p \sim I_P^{-1} (I_P/N)^{-1} T_{e0}$. As a result, $\beta_p = 0.14\, a^{-0.23} I_P^{0.05} (I_P/N)^{-0.56} \Theta^{1.47}$ is obtained under the following assumption for ion temperature: $T_i = T_{e0}$, as shown in FIG. 1(a). Note that β_p shows a weak dependence on I_P, and a decaying tendency with I_P/N that is consistent with that of other RFP plasmas [12]. β_p in TPE-1RM is consistently smaller than the scaling values. This is because $T_i > T_{e0}$ in TPE-1RM, and thus the plasma pressure is underestimated when $T_i = T_{e0}$ is assumed.

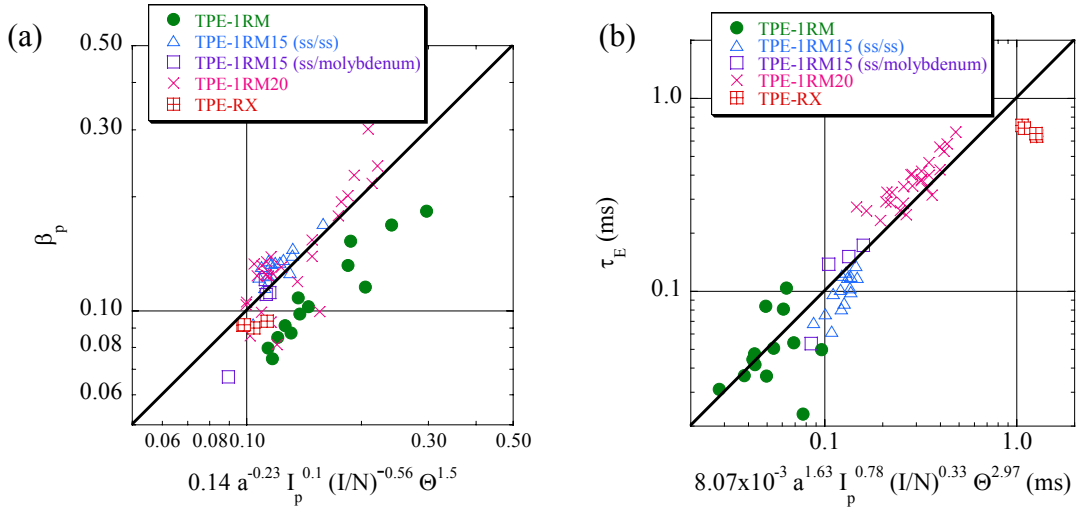

FIG. 1. Regression analysis of (a) β_P, and (b) τ_E for the selected TPE database. Stainless steel (ss) liner and molybdenum limiter are used as the first wall material, except for ss limiter case in TPE-1RM15.

Since the plasma resistance may not yield to Spizter's resistivity, the scaling result of T_{e0} cannot be substituted into the definition of τ_E, and therefore the scaling of τ_E is directly determined as $\tau_{E\_scaling} = 8.07\text{x}10^{-3}\ a^{1.63}\ I_P^{0.78}\ (I_P/N)^{0.33}\ \Theta^{2.97}$, as shown in FIG. 1(b). Also, note that the τ_E values for TPE-RX are below the fitted line. This might be partly due to the presence of the locked modes [13] which did not appear in previous devices. However, the difference is within the standard deviation of all data, and thus TPE-RX data is equally treated in the regression analysis. The τ_E scaling law, except for the Θ dependence, is similar to that theoretically predicted for the transport governed by tearing instabilities [6]. It is noted that both β_p and $\tau_{E\_scaling}$ have a strong increasing tendency with Θ that is spontaneously obtained in the TPE RFPs.

It should be noted here that β_p scaling shows a slightly negative dependence on the plasma size (a). This apparent but weak decrease of β_p with increasing a may be caused by an insufficient power input density as plasma size increases. In order to confirm whether the power input density is insufficient, auxiliary heating using the neutral beam for TPE-RX is planned, and the β-limit will be investigated. A preliminary neutral beam injection using a neutral beam injection (NBI) system, at 0.4 MW with 15 ms duration, was conducted for the first time in the TPE-RX RFP [14]. In spite of the low beam power, a slight increase of I_{SXR} was indicated in some discharges. For a higher power injection, another new NBI system providing an injection of 25 kV, 50 A, and 30 ms duration has been developed. Figure 2 shows the time evolution of the extracted ion beam power (obtained maximum power is much higher than the design value). The beam of these NBI systems is focused at the port position by using concave-type electrodes to pass through a narrow porthole of the vacuum vessel. It is estimated that the beam is focused to have a diameter of 20 mm (the electrode diameter is 345 mm) at the focal point, a high-power-density neutral beam of more than 3 GW/m^2 is produced at the focal point; however, the precise measurement of the beam profile is still being performed.

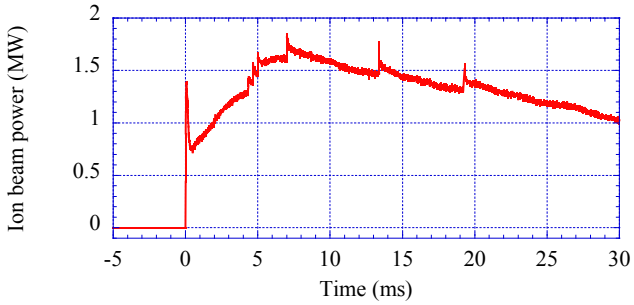

FIG. 2. Time evolution of ion beam power.

3. Characteristics and Empirical Scaling Law of PPCD

3.1. Five-Pulse PPCD Characteristics in TPE-RX

Using a double-pulse operation in PPCD, a fivefold improvement of τ_E was achieved, as shown in ref. 15. Currently, five-pulse operation is possible when using an additional power supply for PPCD. During the five-pulse PPCD operation, the surface-parallel electric field, $E_{//}(a) = [E_\theta(a)\ B_\theta(a) + E_\phi(a)\ B_t(a)]/B$ [16], which confirms the importance of driving the parallel electric field in the edge plasma region, is kept positive for longer period (FIG. 3(a)). Here, E_θ and E_ϕ are the surface poloidal and toroidal electric fields, respectively, and B is the strength of the surface magnetic field. The rate of increase of the soft X-ray (SXR) signal, I_{SXR}, becomes maximum as the poloidal voltage, V_P, becomes maximum (FIGs. 3(a) and (b)).

The value obtained for I_{SXR} suggests that the maximum confinement in the case of five-pulse PPCD operation is higher than that in the case of double-pulse operation (FIG. 3(b)). The confinement properties in the five-pulse PPCD are being measured at present.

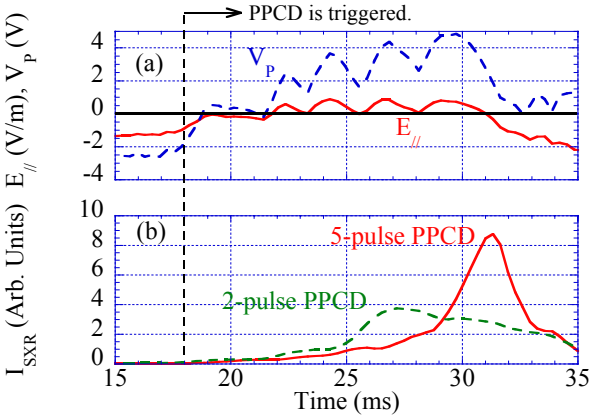

FIG. 3. Time evolutions of (a) $E_{//}(a)$ and V_P in the case of five-pulse PPCD operation and (b) I_{SXR} in cases of five-pulse PPCD operation (solid line) and double-pulse PPCD operation (broken line).

We analyse the systematic scan data under the three sets of operating conditions necessary to obtain higher five-pulse PPCD operation performance in the case of I_P = 350 kA. Figure 4 shows that the I_{SXR} peak increases as the triggering duration of each pulse ($\Delta\tau_{PPCD}$; the time delay between the first and last PPCD pulses) decreases (FIG. 4(a)), as the deuterium gas filling pressure (P_{D2}) decreases (FIG. 4(b)), and as the impurity influx represented by the line intensity of oxygen V ($<I_{OV}>$) decreases (FIG. 4(c)) [17]. In order to take into consideration the overall effect of PPCD, time averaging is conducted between t = 18 ms and 4 ms after the last PPCD pulse which is denoted by <>.

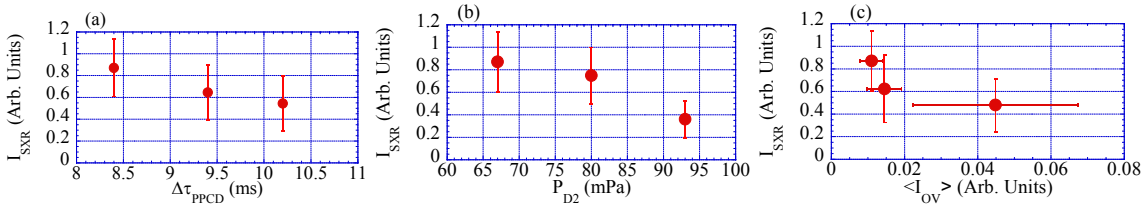

FIG. 4. Correlations between shot-averaged I_{SXR} peak and (a) $\Delta\tau_{PPCD}$, (b) P_{D2} and (c) $<I_{OV}>$.

A statistical analysis shows that I_{SXR} has a clear positive correlation with time-averaged $E_{//}(a)$ over the PPCD phase (FIG. 5(a)). Even if the experimental conditions are the same, in 20% of the shots, the maximum I_{SXR} of PPCD is comparable to that of the standard discharges. The PPCD discharges with the I_{SXR} peak before t = 28.5 ms are called type-B, while the others are called type-A, as shown in FIGs. 5(a) and (b). We found that type-B discharges arise due to an instability in the m = 0, n = 1 magnetic mode, as shown in FIG. 5(c). m and n are the poloidal and toroidal magnetic mode numbers, respectively. The phase- and wall-locking of magnetic modes to the shell gap position might be related to the generation of a larger m = 0 mode in the case of I_P = 350 kA [18].

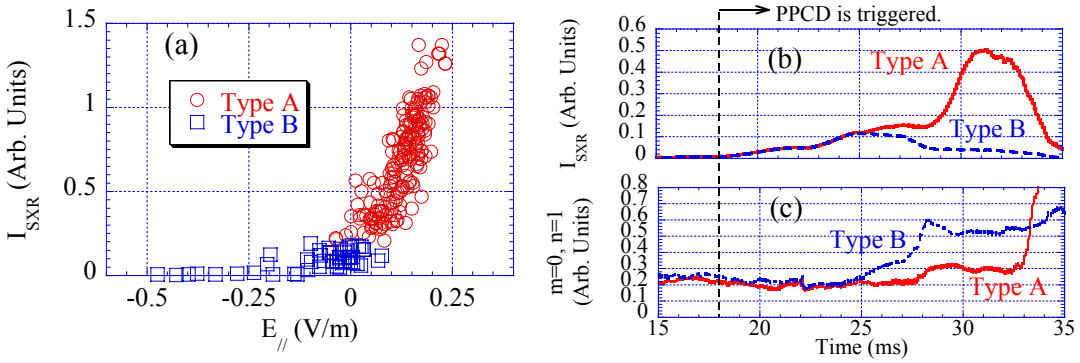

FIG. 5. (a) I_{SXR} correlation with time-averaged $E_{//}$(a), shot-averaged time evolutions of (b) I_{SXR} and (c) m = 0, n = 1 mode.

3.2. Empirical Scaling Law in PPCD

On comparing the scaling law ($\tau_{E\_scaling}$) obtained from the TPE database with the improved confinement, τ_{E_PPCD}, obtained from the PPCD database [7,15,16,19-21] in FIG. 6, we see that the τ_{E_PPCD} values agree well with the values predicted using the TPE scaling law because of its strong dependence on Θ [9]. The least-mean square fit yields $\tau_{E\_PPCD} \sim 0.84\ \tau_{E\_scaling}$. Namely, the improved values obtained in the PPCD experiments are well extrapolated by TPE scaling. Here, the plasma properties for τ_{E_PPCD} and $\tau_{E\_scaling}$ at the time when τ_E has a peak in PPCD are adopted, where they are available in the literature. Note that in PPCD, both /*F*/ and Θ increase transiently. The key element in PPCD, however, is to actively suppress the tearing instabilities in the high-Θ (high magnetic shear) region, in which the core resonant tearing instabilities will otherwise grow, as the current profile is peaked.

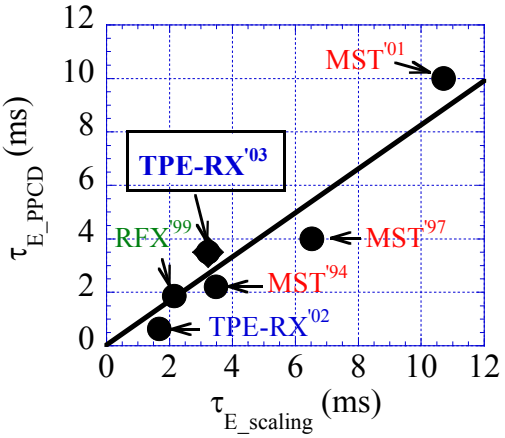

FIG. 6. Comparison of τ_E in PPCD and scaled values.

4. Characteristics of QSH State

4-1. Appearance conditions of QSH State

Since the QSH was first observed in TPE-1RM20 [22,23], QSH states have been detected in a number of RFP devices. QSH states have potential for confinement improvement compared with the multiple helicity (MH) state. To analyse the QSH properties, an extensive set of 436 discharges has been conducted with I_P in the range from 200 to 400 kA and F in the range

from –0.01 to –0.4, and we obtained a two-dimensional map of the probability of QSH appearing [10]. All the shots are characterized by conventional operations with $n_e \sim 6 \times 10^{18}$ m^{-3}, and P_{D2} was 0.4 mTorr. Data from different discharges have been sampled at a time interval corresponding to the flat top of the discharge, where variations of I_P and F are minimal. This time interval is between 25 and 55 ms sampled at steps of 0.5 ms (70-90 ms being the typical discharge duration). In this way, the total number of points is 26160, which corresponds to 436 different discharges. The result shown in FIG. 7(a) indicates that the QSH spontaneously appears with higher probability in the high-I_P and low-/F/, and low-I_P and high-/F/ regions. Here, the QSH state is defined as being that in which the spectral spread number, N_S, introduced in ref. 10, is less than 3. Figure 7(b) displays a contour plot of two-dimensional probability, $P_{QSH}(I_P,F)$, which is defined in ref. 10. P_{QSH} has been interpolated among 12 statistical ensembles marked by white boxes in FIG. 7(b), which are obtained grouping the whole I_P-F plane of FIG. 7(a). P_{QSH} is ~20% at $F\sim$ -0.3 and I_P = 200 kA, while it is ~15% at $F\sim$ -0.05 and I_P = 300 kA. Recently, after increasing the energy in the toroidal reversal bank systems, long lasting QSH state has been observed in the case of $F\sim$ 0 and I_P ~ 200 kA.

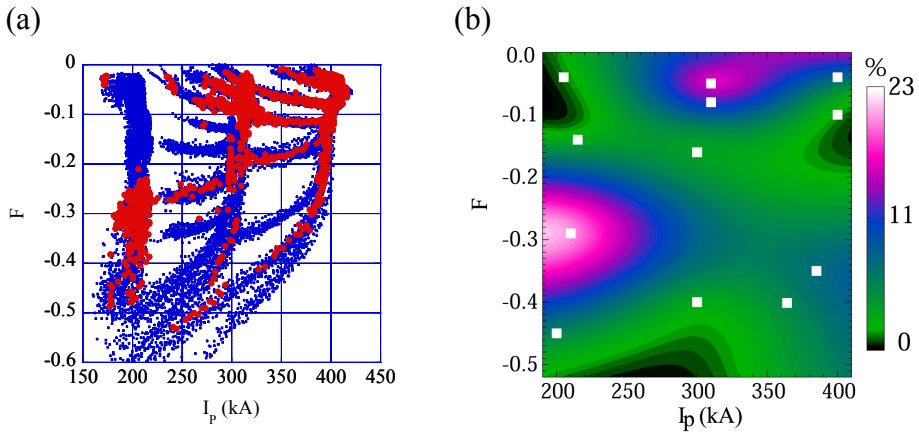

FIG. 7. (a) Experimental coverage in the I_P-F plane (red and blue dots correspond to QSH and MH states, respectively), (b) probability of getting QSH expressed as percentage in the I_P-F plane.

The two basins of high QSH probability differ for the time history of the dominant mode. In FIG. 8(a), toroidal magnetic fluctuation amplitudes of m = 1, n = 6–9 are plotted in the case of I_P = 400 kA. A single n = 6 mode dominates the magnetic m = 1 spectrum starting at t ~20 ms and lasting as long as until the end of the discharge. On the contrary, in the case of low-I_P and high-/F/ discharges, the dominant mode of n = 7 is often interrupted by discrete dynamo events, in which the amplitude of the dominant mode decreases and those of secondary modes increase, as shown in FIG. 8(b).

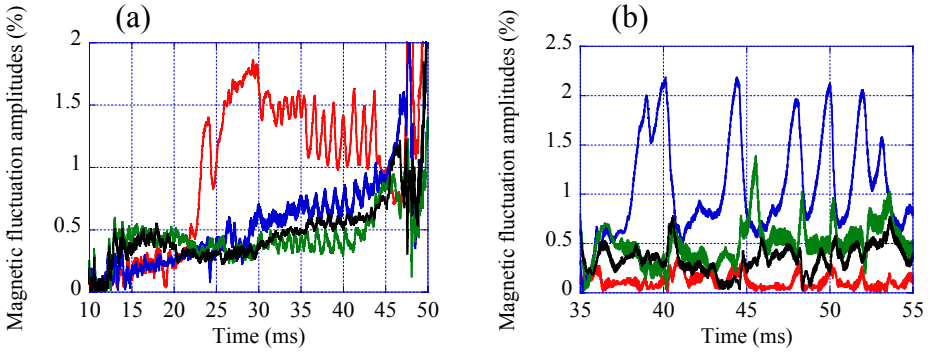

FIG. 8. Time evolutions of the magnetic fluctuation amplitudes (red n=6, blue n=7, green n=8 and black n=9) in the case of (a) I_P = 400 kA and (b) I_P = 200 kA.

4-2. Tomographic Imaging of QSH State

To measure the helical coherent structure in the plasma core, an SXR tomographic imaging system having the same geometrical helicity as the dominant magnetic mode was developed [24]. The system consists of two surface barrier diode (SBD) arrays with15-μm-thick Be-foil. Thirteen SBDs are installed on the vertical ports for measurements along the vertical line of sight, and eleven SBDs are installed on the horizontal port for measurements along a fan-shaped line of sight, as shown in FIG. 9(a). The normalized impact parameters of the lines of sight lie between r/a = -0.80 and 0.80 for the vertical chords, and between r/a = -0.614 and 0.614 for the horizontal chords. Figure 9(b) shows that a clear localized m = 1, n = 6 QSH island structure was observed in SXR tomography, where it is likely that closed flux surfaces were formed. Since in TPE-RX, the modes are usually wall-locked shortly after the beginning of the discharge, the helical island structure does not rotate.
The periodic oscillations of the SXR signal are observed by SXR tomographic imaging. It is found that this SXR oscillation strongly correlates with the oscillation of the m = 0, n = 0 magnetic mode. The helical m = 1 structure disappears when the m = 0, n = 0 magnetic fluctuation grows [25].

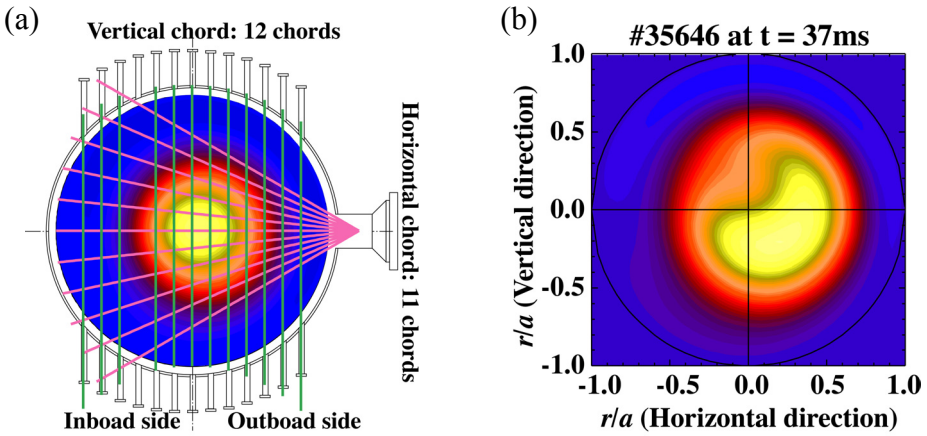

FIG. 9. (a) Schematic drawing of SXR tomography system, and (b) emissivity profile of the SXR in the case of I_P = 300 kA.

5. Summary

TPE-scaling was obtained from the TPE database for four TPE RFP devices under the standard operating conditions that are characterized by relatively high I_P/N values ranging from 5 to 40 x 10^{-14} Am. β_p scaling of $\beta_p = 0.14\ a^{-0.23}\ I_P^{0.05}\ (I_P/N)^{-0.56}\ \Theta^{1.47}$ is obtained under the assumption of ion temperature $T_i = T_{e0}$; note that β_p shows a weak dependence on I_P, and its decaying tendency with I_P/N is consistent with that of other RFP plasmas. The scaling of τ_E yields $\tau_{E\_scaling} \sim a^{1.63}\ I_P^{0.78}\ (I_P/N)^{0.33}\ \Theta^{2.97}$, which shows a weaker dependence on a, I_P and I_P/N than in the constant-β_p scaling case and a strong positive dependence on Θ, and may scale similarly to the scaling of tearing-driven transport. We have shown that TPE-scaling ($\tau_{E\_scaling}$) agrees fairly well with τ_{E_PPCD} in the PPCD database. This is because TPE-scaling has a strong dependence on Θ. The key element in PPCD is to actively suppress tearing instabilities in the high-Θ region. We presented experimental trends indicating the operating conditions necessary to achieve high performance in the five-pulse PPCD. Shorter $\Delta\tau_{PPCD}$, lower P_{D2}, good wall conditions and positive $E_{//}$ are necessary. Suppression of the m = 0, n = 1 magnetic mode instability is also important. The value obtained for I_{SXR} suggests that the

maximum confinement in the case of five-pulse PPCD operation is higher than that in the case of double-pulse operation. In order to investigate the β-limit in RFP, an NBI system with high power density has been successfully developed. The QSH, which has the potential for improved confinement, spontaneously appears with higher probability in the high-I_P and low-/*F*/, and low-I_P and high-/*F*/ regions. In the case of high-I_P and low-/*F*/, a single $n = 6$ mode dominates the magnetic $m = 1$ spectrum starting at $t \sim 20$ ms and lasting as long as until the end of the discharge. On the contrary, in the case of low-I_P and high-/*F*/ discharges, the dominant mode of $n = 7$ is often interrupted by discrete dynamo events. A typical helical island structure was observed by SXR tomography in the QSH state. QSH appears to be a common phenomenology in RFP plasmas as one of the conspicuous features of MHD activities.

This study was financially supported by the Budget for Nuclear Research of the Ministry of Education, Culture, Sports, Science and Technology, based on the screening and counseling by the Atomic Energy Commission.

References

[1] DI MARCO, J., Internal Report Los Alamos National Laboratory, LA-UR-revised-88-3375 (1988).
[2] HOKIN, S., et al., Proc. 22nd Eur. Phys. Conf. on Control. Fusion and Plasma Phys., **19C**, Part I, Bournemouth (1995) 181.
[3] WERLEY, K.A., et al., Nucl. Fusion **36** (1996) 629.
[4] CONNOR, J.W. and TAYLOR, J.B., Phys. Fluids **27** (1984) 2676.
[5] SCHEFFEL, J. and SCHNACK, D., Nucl. Fusion **40** (2000) 1885.
[6] DIAMOND, P.H., et al., Internal Report Oak Ridge National Laboratory, ORNL/TM-9306 (1984).
[7] SARFF, J.S., et al., Phys. Rev. Lett. **78** (1994) 3670.
[8] YAGI, Y., et al., Nucl. Fusion **43** (2003) 1787.
[9] YAGI, Y., et al., "An empirical scaling law for improved confinement in reversed-field pinch plasmas", submitted to Nucl. Fusion.
[10] PIOVESAN, P., et al., Phys. Plasmas **11** (2004) 151.
[11] HIRANO, Y., et al., Nucl. Fusion **36** (1996) 721.
[12] SAKAKITA, H., et al., Jpn. J. Appl. Phys. **43** (2004) 1184.
[13] YAGI, Y., et al., Phys. Plasmas **6** (1999) 3824.
[14] SAKAKITA, H., et al., Proc. 30th Eur. Phys. Conf. on Control. Fusion and Plasma Phys., **27A**, St Petersburg (2003) P2.173.
[15] YAGI, Y., et al., Phys. Plasmas **10** (2003) 2925.
[16] CHAPMAN, B.E., et al., Phys. Rev. Lett. **87** (2001) 205001.
[17] FRASSINETTI, L., et al., J. Phys. Soc. Jpn. **72** (2003) 3297.
[18] FRASSINETTI, L., et al., Bulletin 46th Annual Meeting of American Phys. Soc. on Plasma Phys., Georgia (2004) in press.
[19] SARFF, J.S., et al., Phys. Rev. Lett. **78** (1997) 62.
[20] BARTIROMO, R., et al., Phys. Rev. Lett. **82** (1999) 1462.
[21] YAGI, Y., et al., Plasma Phys. Control. Fusion **44** (2002) 335.
[22] BRUNSELL, P.R., et al., Phys. Fluids **B5** (1993) 885.
[23] HIRANO, Y., et al., Plasma Phys. Control. Fusion **39** (1997) 393.
[24] KOGUCHI, H., et al., Rev. Sci. Instrum. (2004) to be published.
[25] KOGUCHI, H., et al., Bulletin 46th Annual Meeting of American Phys. Soc. on Plasma Phys., Georgia (2004) in press.